Prediction of Supercritical Ethane Bulk Solvent Densities for Pyrazine Solvation Shell Average Occupancy by 1, 2, 3, and 4 Ethanes: Combined Experimental and ab Initio Approach

Bruce J. Hrnjez,*,† Samuel T. Sultan, Georgiy R. Natanov, David B. Kastner, and Michael R. Rosman

Department of Chemistry, Yeshiva University, New York, New York 10033

Received: July 27, 2005; In Final Form: September 20, 2005

We introduce a method that addresses the elusive local density at the solute in the highly compressible regime of a supercritical fluid. Experimentally, the red shift of the pyrazine n−π* electronic transition was measured at infinite dilution in supercritical ethane as a function of pressure from 0 to about 3000 psia at two temperatures, one close (35.0 °C) to the critical temperature and the other remote (55.0 °C). Computationally, stationary points were located on the potential surfaces for pyrazine and one, two, three, and four ethanes at the MP2/6-311++G(d,p) level. The vertical n−π* ($^1B_{3u}$) transition energies were computed for each of these geometries with a TDDFT/B3LYP/6-311++G(d,p) method. The combination of experiment and computation allows prediction of supercritical ethane bulk densities at which the pyrazine primary solvation shell contains an *average* of one, two, three, and four ethane molecules. These density predictions were achieved by graphical superposition of calculated shifts on the experimental shift versus density curves for 35.0 and 55.0 °C. Predicted densities are 0.0635, 0.0875, and 0.0915 g cm^{-3} for average pyrazine primary solvation shell occupancy by one, two, and three ethanes at both 35.0 and 55.0 °C. Predicted densities are 0.129 and 0.150 g cm^{-3} for occupancy by four ethanes at 35.0 and 55.0 °C, respectively. An alternative approach, designed to "average out" geometry specific shifts, is based on the relationship $\Delta\nu = -23.9n$ cm^{-1}, where n = ethane number. Graphical treatment gives alternative predicted densities of 0.0490, 0.0844, and 0.120 g cm^{-3} for average pyrazine primary solvation shell occupancy by one, two, and three ethanes at both 35.0 and 55.0 °C, and densities of 0.148 and 0.174 g cm^{-3} for occupancy by four ethanes at 35.0 and 55.0 °C, respectively.

Introduction

We understand rather well the forces that connect atoms within molecules; our ability to compute gas-phase equilibrium geometries to a high degree of accuracy is evidence of this. We also understand the forces between molecules. In principle, therefore, we should have an understanding of solvation and solvent effects that has predictive value. We do not have this, at least in a form that is useful to the typical experimentalist. The problem, of course, is one of number. As noted by Cramer and Truhlar,[1] if we computationally "treat 200 molecules of a solvent explicitly, this adds 1,800 degrees of freedom for water, 9,000 degrees of freedom for ethyl ether, and 16,200 degrees of freedom for *n*-octanol." The well-reasoned response to this problem is to treat the surrounding solvent as a continuum, and such models are remarkably successful. Yet too often these models fail, especially in cases where dispersion forces dominate the interaction potential between solute and solvent.[2] Explicit treatment of the primary solvation shell is often essential.

Experimentally, the traditional approach[3] to the study of solvent effects is to change the solvent and measure the response of the system. Consequently, we have an enormous body of empirical data that affords the adage "like dissolves like". This ostensibly simple statement has far-reaching implications but falls far short of the quantitative predictive value we seek. The traditional approach leads to correlations of observed solute behavior with bulk solvent properties such as dielectric constant and viscosity. Though useful, these correlations have limited value because a change in solvent involves far more than a mere change in bulk solvent properties. A change in solvent necessarily involves a change in the discrete interactions between solute and solvent molecules. Hence, a solvent change constitutes a change in a multitude of variables, and it is difficult to extract predictive value from experiments in which many variables change simultaneously.

We believe that we can circumvent, or at least mitigate, the multivariable problem by using supercritical fluids as *tools to probe solvent effects*.[4] Typically, a given chemical or physical process can be studied in the fluid of interest at constant temperature slightly above the critical temperature (T_C) as a function of pressure and, therefore, density of the medium. Operation above T_C precludes the complication of a gas−liquid phase change, and the density of the medium can be varied continuously from gaslike to liquidlike. Bulk solvent properties such as dielectric constant and viscosity vary predictably with density, while the types of intermolecular interactions available to solute and solvent remain constant. We can therefore study solvent effects *without changing the solvent*.

There is, however, a complication that must be resolved if we are to make use of this tool. It is now well recognized[5,6] that in a supercritical fluid, the local solvent density in the immediate vicinity of a solute deviates from the bulk solvent density in the highly compressible regime where the bulk solvent property change is greatest. In fact, for the majority of cases in which the attractive interaction potential between solute and solvent molecules is lower in energy than that between solvent molecules, the local density in the immediate vicinity of the

* Address correspondence to this author. E-mail: hrnjez@yu.edu.

† This paper is respectfully dedicated to Alex Nickon, Vernon K. Krieble Professor Emeritus of Chemistry at Johns Hopkins University.

10.1021/jp054150d CCC: $30.25
Published on Web 10/26/2005

solute is greater than the solvent bulk density in the highly compressible regime. If the solvent number density in the solute primary solvation sphere cannot be approximated by the bulk solvent number density, then the local dielectric and viscosity are not the same as the bulk values. Unfortunately, the detailed physical picture is not well understood,[7−20] and the tool therefore lacks predictive value in the region of greatest interest. So, if we wish to use supercritical fluids as tools to study solvent effects (and we do), then the local density physical picture must be refined. This paper represents our initial attempt to contribute to a better practical understanding of the clustering phenomenon, sometimes known as local density augmentation or enhancement, in the highly compressible regime of supercritical fluids.

Experimentally, we measured the *red* shift of the pyrazine n−π* electronic transition in supercritical ethane as a function of pressure from 0 to about 3000 psia at two temperatures, one close (35.0 °C) to T_C and the other remote (55.0 °C) from T_C. Computationally, we located stationary points on the potential surfaces for pyrazine and one, two, three, and four ethanes at a modest level of quantum-chemical theory, using the second-order Møller−Plesset perturbation[21] (MP2) method and the 6-311++G(d,p)[22] medium-sized basis set. We then computed the vertical n−π* ($^1B_{3u}$) transition energies for each of these geometries with a time-dependent density functional[23] (TDDFT) method using the hybrid Becke-style 3-parameter density functional theory (DFT) with the Lee−Yang−Parr correlation functional[24] (B3LYP) and the same medium-sized basis set, which is a method well documented by Weber and Reimers[25] to reliably produce excitation energies for pyrazine that agree with experiment. The combination of experiment and computation allows us to predict supercritical ethane bulk densities at which the pyrazine primary solvation sphere contains an average of one, two, three, and four ethane molecules.

Toward defining a pyrazine−ethane potential that will be useful for eventual molecular simulation, we further focused computationally on our lowest energy structure for pyrazine and one ethane. We refined this structure by optimizing in the presence of the counterpoise correction.[26] A subsequent frequency calculation yielded the zero-point vibration and thermal energy corrections to total energy and allowed identification of a low-frequency vibrational mode for which pyrazine and ethane are most strongly coupled. We explored the potential surface of this refined structure in two dimensions as a function of pyrazine−ethane distance and rotation of ethane with respect to pyrazine. Calculation of the vertical electronic transition energies at each of the points on these two surfaces gives insight into the sensitivity of the transition energy to movement of ethane within the shallow potential well. Finally, we calculated the single-point energy of the refined structure at the MP2 level of theory with a large basis set (aug-cc-pVQZ)[27] known to be near the basis set limit for van der Waals clusters of this type.[28,29] We thereby evaluate the approximation inherent in our general use of the truncated 6-311++G(d,p) basis set.

We chose our system, pyrazine in ethane, for several reasons. The solute, pyrazine, is a planar, cyclic, six-membered, aromatic 1,4-diazine (see Figure 1) that is well known to the computational community.[25] It is a popular molecule used to test a variety of theoretical models. Its crystal structure is known.[30] The structural parameters are known also from a combined electron diffraction, liquid-crystal NMR, and rotational data method.[31] Pyrazine is well studied spectroscopically.[32−35] The vibrational structure of the n to π* electronic transition remains well resolved even at liquidlike densities, allowing unambiguous experimental focus on the 0−0 transition. It is easily obtained

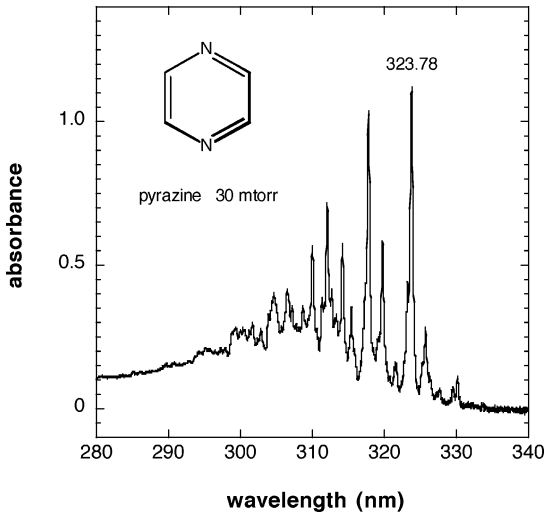

Figure 1. Gas-phase (30 mTorr) UV spectrum of the pyrazine n−π* transition (0−0 band maximum at 323.78 nm).

in high purity, and it is a low-melting solid with high vapor pressure at room temperature.[35] Solvent clustering around pyrazine ions has been studied in supercritical ethane.[36] Pyrazine derivatives are biologically relevant.[37] The solvent, ethane, is a simple organic molecule that yet retains the interest of computational chemists, as evidenced by Goodman's compelling assertion[38] that the staggered conformational preference is the result of hyperconjugative stabilization. Ethane is a simple model for hydrocarbon solvation. The critical parameters are convenient (T_C = 32.15 °C, P_C = 710.5 psia, critical density = 0.207 g cm^{-3}), and it is also available in high purity. Supercritical ethane is of practical interest in separation technology and as a reaction medium.[39,40]

Central to our system choice was our expectation that dispersion forces dominate the interaction between pyrazine and ethane. At this stage in our development of a tool to probe solvent effects, it is important that we minimize the complexity of an already complex system. We therefore focus our attention on a system in which a single solvation mode predominates, one that is adequately modeled only by quantum mechanical methods that involve electron correlation and large basis sets.[28] Dispersion dominance is not self-evident; Tsuzuki[29] showed that the orientation dependence of the methane−benzene interaction is electrostatic, but small (17%) compared to the long-range dispersion component of the total (−1.45 kcal mol^{-1}) calculated at the coupled cluster singles and doubles with triples correction[41] (CCSD(T)) limit.

We report (1) the experimental UV absorbance behavior of the supercritical ethane−pyrazine system, (2) the quantum-chemically determined structures for pyrazine and one, two, three, and four ethanes, (3) the computed n−π* transition energies of these structures, (4) our prediction of the supercritical ethane densities at which the pyrazine primary solvation sphere contains an average of one, two, three, and four ethanes, and (5) a two-dimensional computational probe of the pyrazine−ethane potential surface and the n−π* transition energy sensitivity to ethane movement on this potential surface.

Experimental Methods

Absorbance measurements were made with a Cary 300 UV−vis spectrophotometer (grating 30 × 35 mm, 1200 lines/mm), which has a limiting resolution rated to less than 0.2 nm. Routine data collection with a 0.2 nm slit width and 0.02 nm data intervals focused on the 0−0 band of the pyrazine n−π*

transition in the region 335−322 nm after we determined that all other well-resolved vibrational bands within the total transition (335−295 nm) showed the same absorbance maximum shift with increasing ethane density. The absorbance maximum for the gas phase 0−0 band was reproducibly 323.78 ± 0.02 nm (literature[34,35] value 323.88 nm) at 30 mTorr before the introduction of ethane into the stainless steel pressure vessel; this maximum was not temperature dependent over the range studied. Experiments were conducted at constant temperature (35.0 or 55.0 ± 0.1 °C) as a function of pressure from 0 to 3000.0 ± 1.3 psia at pressure intervals as small as 5 psia in the highly compressible regime. Each of the two reported data sets (35 and 55 °C) is a composite of several data sets, from which many points have been omitted to improve presentation clarity without compromising any indication of scatter in the data. Ethane densities (±0.2%) were calculated with an equation of state[42] used for on-line calculation of fluid properties by the National Institute of Standards and Technology (NIST) Chemistry WebBook service.[43]

Pyrazine (>99%) was purchased from Aldrich Chemical Co. and used without further purification, although we did take advantage of the fact that pyrazine readily sublimes at room temperature and atmospheric pressure. That is, we routinely used material that had sublimed to the upper walls of the storage bottle. Ethane (UHP Grade) was purchased from Matheson Tri-Gas and used without further purification.

The stainless steel pressure vessel was either a two- or four-windowed (sapphire, ISP Optics) assembly, custom built by Parr Instrument Company. Window seals were flexible graphite. The desired amount of ethane was introduced into this optical vessel and the pressure manipulated with a syringe pump (High Pressure Equipment Company, 60 cm^{-3} capacity, rated to 5000 psia) fitted with Teflon packing. Connections were made with stainless steel valves, fittings, and tubing, also obtained from High Pressure Equipment Company. Pressure was measured with a digital pressure indicator (Heise, model PM, range 0 to 5000 psia, with 0.025% full scale accuracy), factory-calibrated with a pressure standard traceable to NIST. The optical vessel temperature was controlled with an Omega Programmable Controller (model CN3004), a thermistor probe (Omega, model TJ72), and two cartridge heaters (250 W) connected to a variable transformer. The thermistor probe was inserted into a stainless steel well in the optical vessel that was close to the fluid region sampled with incident light. This hardware constitutes a "system" that was mounted on a wheeled cart with a 24 × 36 in. working surface.

Because machined stainless steel materials are often contaminated with machining oils, special care was taken to rigorously clean all surfaces that contact fluid. All components were rinsed copiously with *n*-hexane (Aldrich, >99%) and then washed with a hot Alconox soap solution (10% (w/v) in distilled water and 0.2 μm filtered). Finally, all surfaces were rinsed copiously with filtered (0.2 μm), hot distilled water. After most of the water had been removed, the entire system was placed under high vacuum for several days and then judged adequate for our purposes. Residual surface hydration of stainless steel surfaces was assumed unlikely to compromise the experiment; our observed gas phase 0−0 band absorbance maximum for pyrazine agrees well with that observed previously.[34,35] The UV spectrum of ethane at high density did not reveal contamination by any UV-absorbing substances in the region of interest.

Pyrazine was loaded reproducibly by introducing a single crystal (ca. 2.0 mg, 2.5 × 10^{-2} mmol) into the open stainless steel optical vessel such that the crystal could easily be observed through one of the sapphire windows. The closed vessel containing the highly volatile pyrazine solid was then evacuated beyond the point at which any solid could be observed with the unaided eye (about 3 min). This typically corresponded to a pressure of about 30 mTorr (2.7 × 10^{-6} psia), as measured by a standard thermocouple vacuum gauge. This initial load pressure gives a constant pyrazine concentration of about 1.6 × 10^{-6} M over the course of a single data collection run at constant temperature as a function of incremental addition of ethane (increasing pressure at constant vessel volume).

Computational Methods

Preliminary ab initio electronic structure calculations for pyrazine, ethane, ethane dimer, and pyrazine with one, two, and three ethanes were performed with Spartan04.[44] Subsequent calculations on these species and on pyrazine with four ethanes were performed with Gaussian03.[45] Electron correlation was modeled at the MP2 frozen-core level for ground-state calculations and at the B3LYP level for excited-state calculations. Program package defaults, including criteria for wave function convergence and locations of stationary points on potential surfaces, were used. Standard basis sets, including 6-311+G-(d), 6-311++G(d,p), and aug-cc-pVQZ, were used without modification. Geometry optimizations for all configurations of pyrazine with one, two, three, and four ethanes were performed in the absence of the counterpoise method. For estimation of the basis set superposition error (BSSE),[46] the counterpoise method was applied to optimized structures. In a single case, final geometry optimization in the presence of the counterpoise method was performed for our configuration in which pyrazine and one ethane are most strongly bound. This resulted in modest refinement of the optimized geometry and a significant increase in the binding energy for the cluster, suggesting that incorporation of the counterpoise method into geometry optimization routines may be important for weakly bound clusters of this type.

Results and Discussion

Our objective is to describe two components of our ongoing study of pyrazine in ethane. The first component is the experimental description of how pyrazine absorbs UV light as a function of ethane density. The second component is the computational description of how pyrazine absorbs UV light as a function of ethane number and orientation with respect to pyrazine. These two components should allow prediction of the experimental densities at which pyrazine is associated with an average of one, two, three, and four ethanes. The second, computational, component also lays the groundwork for the construction of pyrazine−ethane and ethane−ethane[47] potentials to be used for molecular dynamics simulation. Given adequate potentials, future simulation studies will afford a means by which we can evaluate the integrity of our density predictions and acquire insight into the width of ethane number distribution at a given density.

Pyrazine in Supercritical Ethane. Current use of the word "supercritical" implies operation above T_C , irrespective of the pressure. Operation above T_C avoids the complication of gas−liquid phase transitions and allows continuous variation in bulk fluid density from gaslike to liquidlike values. Our starting point, therefore, is pyrazine in the absence of ethane. The well-resolved spectrum for the gas-phase n−π^* transition for pyrazine is shown in Figure 1. The principal features of this spectrum remain resolved even at the highest ethane density studied (ca.

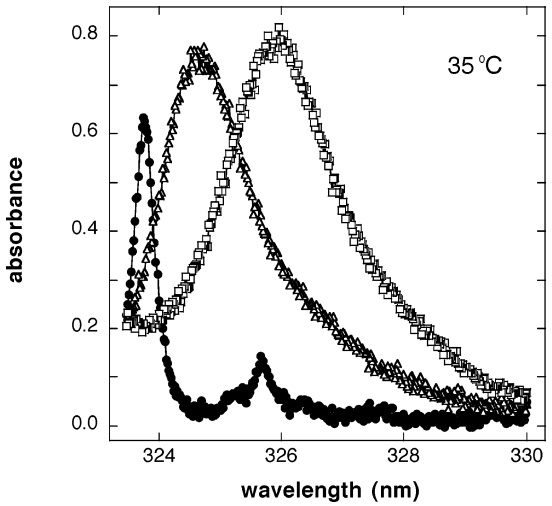

Figure 2. Red shift of the 0−0 band of pyrazine n−π* transition as a function of pressure from 0 to 3120.5 psia at 35.0 °C. Representative data at 0 (filled circles, λ_{max} = 323.78 nm), 720.3 (open triangles, λ_{max} = 324.66 nm), and 3120.5 psia (open squares, λ_{max} = 325.96 nm).

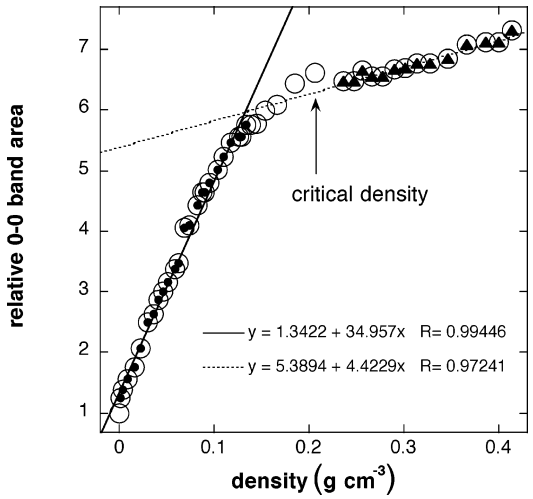

Figure 3. Relative area of the pyrazine n−π* transition 0−0 band as a function of ethane bulk density at 35.0 °C (open circles). Apparently linear low-density region (fit, solid line) from 0.00125 to 0.134 g cm^{-3} (small filled circles). Apparently linear density region (fit, dashed line) from 0.236 to 0.414 g cm^{-3} (small filled triangles).

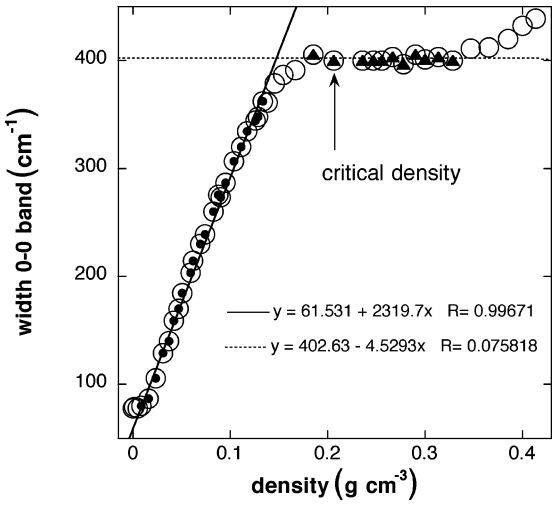

Figure 4. Width of the pyrazine n−π* transition 0−0 band as a function of ethane bulk density at 35.0 °C (open circles). Apparently linear low-density region (fit, solid line) from 0.00868 to 0.134 g cm^{-3} (small filled circles). Apparently linear medium-density region (fit, dashed line) from 0.207 to 0.328 cm^{-3} (small filled triangles).

0.4 g cm^{-3}) and shift uniformly to the red with increasing ethane density. We focused on the 0−0 band indicated at 323.78 nm. Figure 2 shows the typical behavior of this band at 35.0 °C and three pressures from 0 to 3120.5 psia. (The behavior at 55.0 °C, not shown, is qualitatively the same.) The 323.78 nm origin at 0 psia is reproducibly at lower intensity (0.62 absorbance units in this case) before the introduction of ethane. A small amount of ethane (ca. 5 psia is sufficient) gives an immediate increase in the band intensity to 0.76 absorbance units and a very small shift of 0.02 nm to the red. Intensity increase continues until about 178 psia, after which the intensity decreases and the band broadens substantially. The band intensity reaches a local minimum at about 740 psia and 325 nm, followed by a modest intensity increase with increasing pressure to a value that remains approximately constant at the higher pressures. The total red shift is 2.18 nm (−206.6 cm^{-1}), which corresponds to a decrease in the n−π* transition energy of 0.59 kcal mol^{-1}.

Since our window seals are flexible graphite, it is conceivable that adsorbed pyrazine from previous trials could account for the observed increase in band intensity with increasing ethane density. However, control experiments reveal that this is not the case. We suggest that the observed intensity increase corresponds to an effect of ethane on the pyrazine n−π* transition oscillator strength, and Figure 3 depicts the change in relative 0−0 band area with density. Meyers and Birge[48] derived a simple expression to account for their experimental observations with pyrazine in a series of hydrocarbon solvents that requires knowledge of the solvent refractive index and a geometric factor that depends on the shape of the solute and the orientation of its transition moment. Even with a simple cylinder model in which the transition moment is perpendicular to the cylinder axis, they achieved good agreement with the experimentally observed increase in oscillator strength with increasing solvent refractive index. We do not apply this expression to this system, but are currently exploring this as a means by which to predict the local refractive index at the solute in the low-density regime of a supercritical fluid.

Figure 2 also reveals a dramatic increase in the width of the 0−0 transition with increasing density. The nontrivial explanation for this effect usually involves the supposition that different local chromophore environments in the condensed phase give a distribution of electronic energy gaps and an ensemble-averaged spectrum that is inhomogeneously broadened.[49] Given the fact that we will eventually compare the observed widths to the distribution of environments we obtain in future simulation experiments, we report the change in the width of the 0−0 transition with density at 35.0 °C in Figure 4.

Both Figures 3 and 4 show strikingly linear behavior for the changes in 0−0 band area and width with increasing density in the low-density regime. Although the initial low-density points for the two low-density linear regions differ slightly, they both terminate at an ethane bulk density of 0.134 g cm^{-3}. These observations suggest that the change in the local density about pyrazine in the low-density regime is rather well-behaved. The plateau region in Figure 4 for the change in width with density is deceptively linear to the eye. In fact, the low correlation coefficient (R = 0.076) may indicate that the system is oscillating with significant amplitude about some local density number.

The translation of the raw data to 0−0 band shift in wavenumbers with respect to pressure at both 35.0 and 55.0

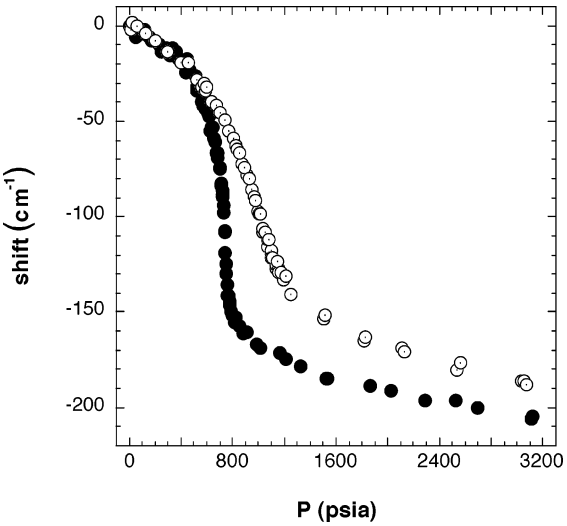

Figure 5. Red shift of the 0−0 band maximum of the pyrazine n−π* transition as a function of pressure from 0 to 3120.5 psia at 35.0 (filled circles) and 55.0 (open circles with center dot) °C.

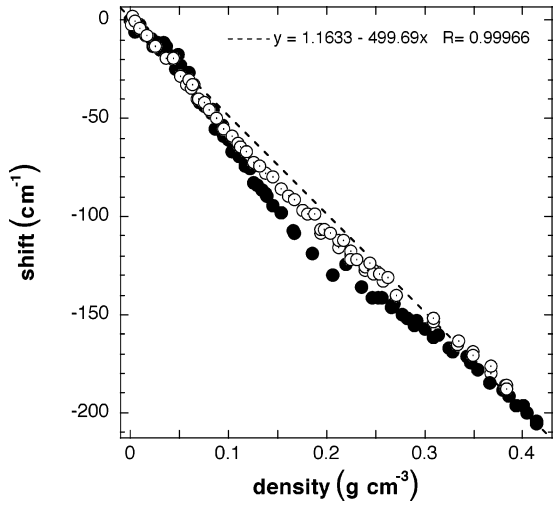

Figure 6. Red shift of the 0−0 band maximum of the pyrazine n−π* transition as a function of ethane bulk density from 0 to 3120.5 psia at 35.0 (filled circles) and 55.0 (open circles with center dot) °C. The dashed line (linear fit shown) is given by apparently linear points at low (0−0.06 g cm^{-3}) and high (0.34−0.42 g cm^{-3}) densities for both data sets.

°C is shown in Figure 5. As anticipated,[5] the majority of the shift at the temperature closer (35.0 °C) to T_C takes place over a much narrower pressure range than at the temperature more remote (55.0 °C). Figure 6 shows the shift with respect to calculated ethane bulk density at both temperatures. The dashed line, defined by the apparently linear regions at low and high densities, may be thought to represent the expected behavior of the system if the local ethane density at pyrazine were equal to the bulk ethane density. The curvatures away from linearity illustrate a well-documented[5,6] aspect of operation close to T_C in a supercritical fluid. Namely, the local solvent density in the immediate vicinity of the solute deviates from the bulk solvent density in the highly compressible regime. The smaller deviation from linearity at the higher temperature reflects decreased importance of the relatively small potential difference between the pyrazine−ethane and ethane−ethane systems. Effectively, the small potential difference between the two systems is swamped by the higher kinetic energies at the higher temperature. One would expect the shift to linearize at sufficiently high temperature; we did not explore the higher temperature

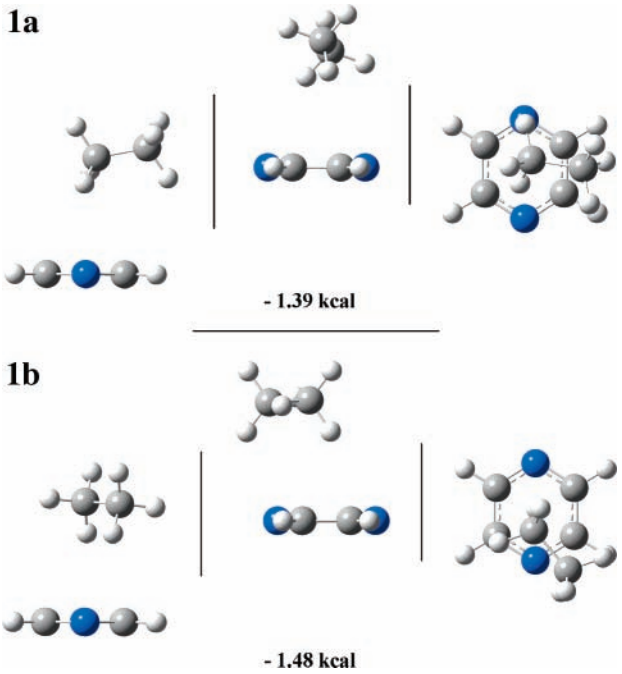

Figure 7. Structures **1a** and **1b** for pyrazine and one ethane. Blue is nitrogen; gray is carbon; and white is hydrogen. Three perspectives are shown: the left structure has the pyrazine plane and the N−N axis perpendicular to the page; the middle structure has the pyrazine plane perpendicular to the page and the N−N axis coplanar with the page; and right structure has the pyrazine plane coplanar with the page.

regime. The region between approximately 0.05 and 0.20 g cm^{-3} is of greatest interest to us at present. One interpretation is that this is the region in which the primary solvation sphere of pyrazine fills stepwise, and the short-range interaction between pyrazine and closely associated ethanes exerts most of the effect on the experimentally observable electronic transition energy.

Pyrazine and Ethane Computational Approach. We make the simplifying assumption that pyrazine's primary solvation sphere fills stepwise with one, two, three, and four ethanes in the low density region. We computationally determined representative structures for pyrazine and one, two, three, and four ethanes (Figures 7−10 and Table 1). We then calculated the n−π* transition energies for each of these structures and determined their shifts with respect to the calculated n−π* transition for isolated pyrazine. Graphical superposition of the calculated shifts on the plot of our experimentally observed shift with respect to ethane density afforded our prediction of the ethane densities at which pyrazine's solvation sphere is dominated by ethane number densities of one, two, three, and four (Figure 11, Table 2).

We relied on simple logic to probe the configuration space in order to determine our two representative structures for pyrazine and one ethane (**1a** and **1b**, Figure 7). We constructed many initial geometries for ethane with respect to pyrazine and then optimized these geometries at the MP2/6-311+G(d,p) level. Monomer geometries within the supramolecular calculations were not held fixed, but were allowed to relax. These initial geometries included several in which the C−C ethane bond was coplanar with the pyrazine atomic plane and close to or remote from nitrogen with its in-plane lone pair of electrons. Initial geometries for ethane above the pyrazine plane included those in which the C−C ethane bond was parallel or perpendicular to the pyrazine plane, and also close to or remote from nitrogen. We also probed relatively large and small initial pyrazine−ethane distance geometries. We eventually obtained 12 inter-

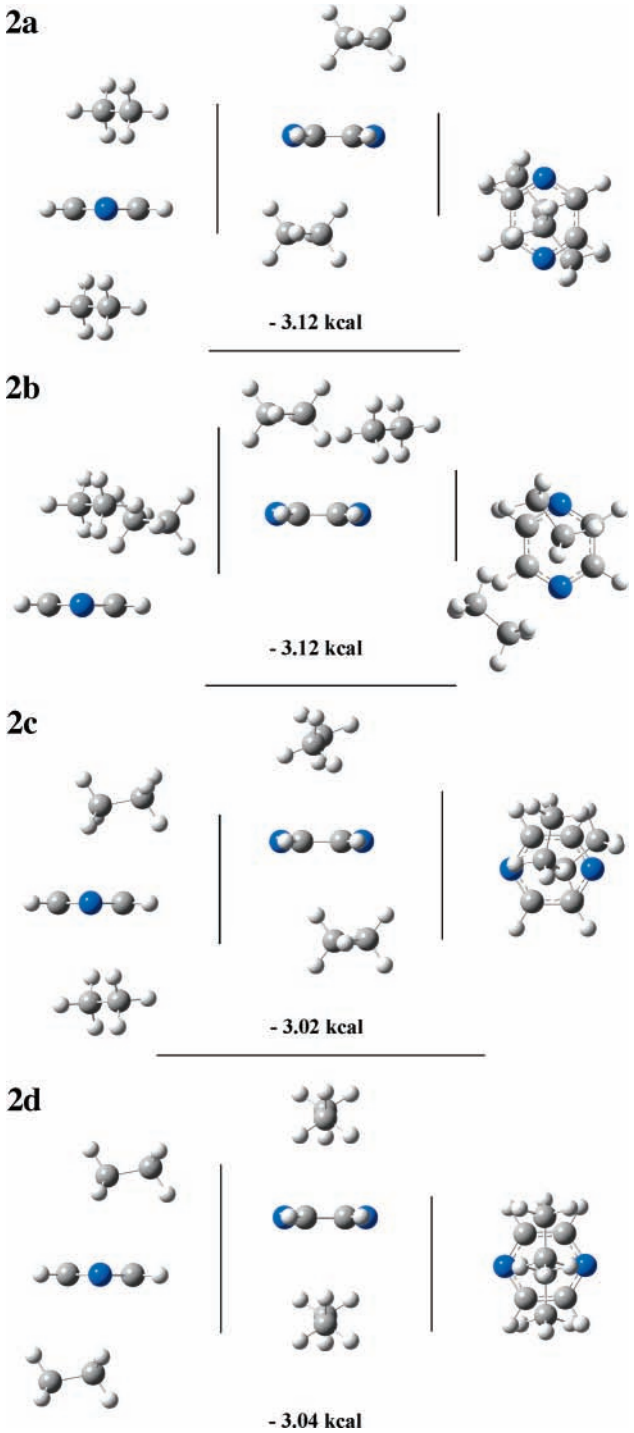

Figure 8. Structures **2a**−**d** for pyrazine and two ethanes. Blue is nitrogen; gray is carbon; and white is hydrogen. Three perspectives are shown: the left structure has the pyrazine plane and the N−N axis perpendicular to the page; the middle structure has the pyrazine plane perpendicular to the page and the N−N axis coplanar with the page; and the right structure has the pyrazine plane coplanar with the page.

mediate structures that we further optimized with the larger 6-311++G(d,p) basis set. All converged to either **1a** or **1b**. We did not find a local minimum corresponding to a structure in which the ethane C−C axis is perpendicular to the pyrazine plane. Nor did we find a local minimum in which an ethane hydrogen is closely associated with a nitrogen lone pair in what could be regarded as a weak hydrogen bonding interaction. We do not claim to have found the global minimum, but we are confident that we have found two representative local minima.

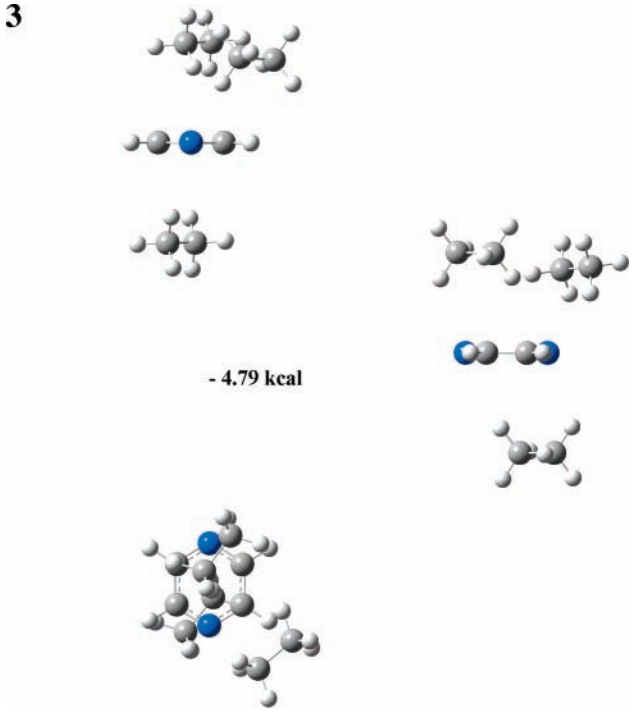

Figure 9. Structure **3** for pyrazine and three ethanes. Blue is nitrogen; gray is carbon; and white is hydrogen. Three perspectives are shown: the top structure has the pyrazine plane and the N−N axis perpendicular to the page; the middle structure has the pyrazine plane perpendicular to the page and the N−N axis coplanar with the page; and the bottom structure has the pyrazine plane coplanar with the page.

Ideally, it would be best to optimize geometries with the large aug-cc-pVQZ basis set to ensure adequate capture of the dispersion component of the pyrazine−ethane interaction, but this is prohibitively expensive when carried to systems as large as pyrazine with four ethanes. Furthermore, there is evidence that the MP2 correlation method overestimates the binding energy for van der Waals clusters and that the CCSD(T) method may be necessary if accurate energies are needed.[28] Tsuzuki recently estimated the CCSD(T) interaction energy for naphthalene dimers at the basis set limit with a technique that included MP2 correlation near saturation and a CCSD(T) correction term determined with a medium-sized basis set.[50] A similar estimation method may eventually be necessary for our system when we construct potentials appropriate for molecular dynamics simulation. We judge that high-level ab initio computations involving CCSD(T) methods are not necessary for the present purposes. We need reasonable structures for the series pyrazine and one, two, three, and four ethanes at reasonable computational cost. Final optimization with the 6-311++G(d,p) basis set, with its diffuse functions on heavy atoms and hydrogen, satisfies this need.

Structures **1a** and **1b** were used to construct four initial structures for geometry optimization of selected pyrazine and two-ethane configurations. Geometry optimization at the MP2/6-311+G(d,p) level was followed by further optimization with the larger 6-311++G(d,p) basis set to afford structures **2a**−**d** (Figure 8). We did not exhaust all possible combinations of **1a** and **1b**. Structure **2b** is the only one of these four in which the two ethanes are on the same side of the pyrazine plane.

The single pyrazine and three-ethane structure (**3**, Figure 9) is a composite of **2a** and **2b**. Likewise, the single pyrazine and four-ethane structure (**4**, Figure 10) is derived from **3**. These structures were also optimized in a stepwise fashion at the MP2 level with the smaller and then the larger basis sets. Given the

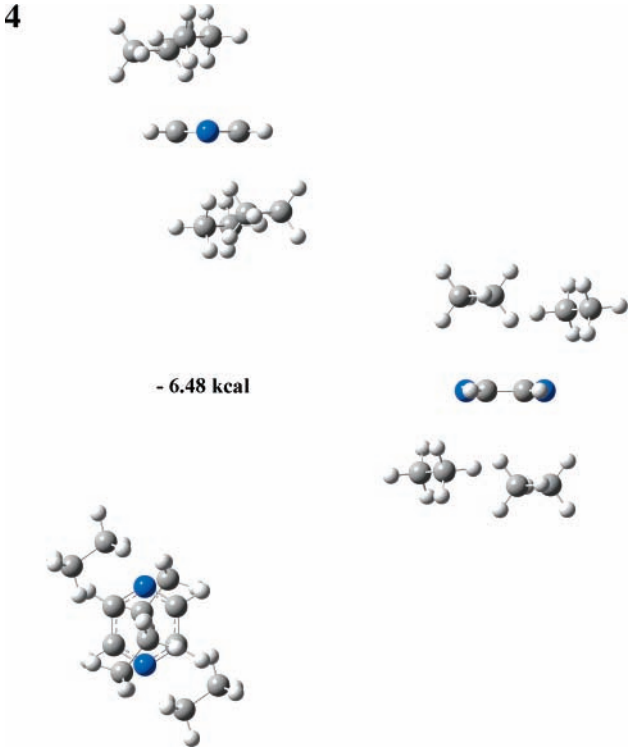

Figure 10. Structure **4** for pyrazine and four ethanes. Blue is nitrogen; gray is carbon; and white is hydrogen. Three perspectives are shown: the top structure has the pyrazine plane and the N−N axis perpendicular to the page; the middle structure has the pyrazine plane perpendicular to the page and the N−N axis coplanar with the page; and the bottom structure has the pyrazine plane coplanar with the page.

high computational cost for the three- and four-ethane cases, we chose to focus on only a single representative for each of these two cases. Counterpoise corrections for **1**−**4** were computed for the fully optimized structures.

Table 1 also gives our results for isolated pyrazine and ethane, for which the equilibrium geometries were calculated by the same method. Calculated pyrazine bond lengths were 1.34295, 1.39443, and 1.08786 Å for C−N, C−C, and C−H, respectively. Those for ethane were 1.52908 and 1.09359 Å for C−C and C−H, respectively. Pyrazine and ethane bond lengths within the supramolecular structures **1**−**4** changed by no more than about 0.005 Å. We report the binding energies for structures **1**−**4**, obtained by subtracting the energies of the isolated species from the total energies of the structures **1**−**4**. A plot of ethane number as a function of binding energy (not shown) gives extremely good linear correlation ($R = 0.9996$). In fact, the binding energy (E_b) as a function of ethane number (n) is reasonably represented by the expression, $E_b = -1.58n$ kcal mol^{-1}. The ethane dimer (two ethane) entry agrees well with published[51] results and is tabulated here as a point of reference for comparison.

Calculation of n−π* Transition. Weber and Reimers[25] evaluated 22 ab initio and density functional schemes for calculating the vertical excitation energies for eight singlet excited states of pyrazine with the cc-pVDZ basis set. Of these, the TDDFT/B3LYP method was among the most reliable; it gave an n−π* transition energy of 3.99 eV. Using this method with the 6-311++G(d,p) basis set gave 3.9464 eV for isolated pyrazine. These values represent average absorption frequencies and may be compared to the 3.97 eV experimental value,[25] which is the sum of the 0−0 transition energy (3.83 eV, 323.82 nm) and the estimated reorganization energy (0.14 eV).[32] We applied this method to the pyrazine and ethane structures **1**−**4** and obtained the results also tabulated in Table 1. The average calculated shifts for **1** and **2** are −34.9 and −50.6 cm^{-1}, respectively. The single value for **3** (−52.6 cm^{-1}) is nearly the same as the average for **2**, whereas the single value for **4** (−83.9 cm^{-1}) represents a substantial relative shift.

These calculated values are not far removed from experimental values obtained by Bernstein[35] in his supersonic molecular jet study of van der Waals clusters of pyrazine with one, two, and three ethanes. He reported three broad features of approximately equal intensity for the pyrazine and one ethane cluster with red shifts of −41.1, −52.5, and −56.3 cm^{-1} (average, −50.0 cm^{-1}). The pyrazine and two ethane cluster showed two intense features (−57.6 and −65.0 cm^{-1}) and a much weaker feature at −41.8 cm^{-1} (average of the two intense features, −61.3 cm^{-1}). The pyrazine and three-ethane cluster showed several features ranging from −40.8 to −72.7 cm^{-1}, but an intense feature at −65.5 cm^{-1} clearly dominated the spectrum. Our small change in calculated shift for **2** and **3** is thereby substantiated by experiment.

Our average calculated shifts and Bernstein's average experimental shifts are shown in Table 2 for comparison. Given the close agreement in magnitude and trend, our graphical density predictions depicted in Figure 11 and given numerically in Table 2 are reasonable. We arrived at these density predictions by visually superposing our average calculated shifts for **1**−**4** on the experimental shift versus density curves for 35.0 and 55.0 °C and then reading the corresponding densities. Because these two curves coincide below a shift of about −55 cm^{-1}, our predicted densities for structures **1**−**3** are equal. At the −83.9 cm^{-1} shift predicted for **4**, we are able to predict two different densities for the two different curves.

Alternatively, the pattern of average coordination number may be more uniform than indicated by the above predictions. In contrast to the binding energies, the calculated shifts show only a moderate linear correlation ($R = 0.838$) when plotted as a function of ethane number (not shown). Even so, this relationship may be used to construct an expression for the shift ($\Delta\nu$) as a function of ethane number (n), which is reasonably represented by $\Delta\nu = -23.9n$ cm^{-1}. This estimate may better "average out" the geometry specific shifts that are a necessary consequence of our limited sampling of pyrazine−ethane structures. A graphical treatment the same as that described above gives alternative predicted densities of 0.0490, 0.0844, and 0.120 g cm^{-3} for average pyrazine primary solvation shell occupancy by one, two, and three ethanes at both 35.0 and 55.0 °C, and densities of 0.148 and 0.174 g cm^{-3} for occupancy by four ethanes at 35.0 and 55.0 °C, respectively.

Refinement of Pyrazine and One-Ethane Structure. Since BSSE is a large component of the calculated binding energies for **1**−**4**, we tested the importance of incorporating the counterpoise method into the geometry optimization scheme rather than merely calculating the BSSE for geometry optimized structures. Accordingly, we selected the structure in which pyrazine and one ethane are most strongly bound, **1b**, and optimized this structure in the presence of the counterpoise method. The result was structure **1c** (not shown), which is a visually indistinguishable modification of the orientation of ethane with respect to pyrazine, but corresponds to a significant change (11%) in the binding energy from −1.48 to −1.65 kcal mol^{-1} for **1b** and **1c**, respectively. A TDDFT/B3LYP/6-311++G(d,p) calculation for **1c** gave the same value for the n−π* transition energy obtained for structure **1a** (3.9431 eV, 314.44 nm) with a shift of −27.3 cm^{-1}. These results suggest that it may be necessary to perform geometry optimizations in

TABLE 1: Calculated Ground State MP2/6-311++G(d,p) Energies and Excited State TDDFT/B3LYP/6-311++G(d,p) Singlet n−π* Transition Energies for Pyrazine and One, Two, Three, and Four Ethanes

system	$E_{electronic}$ (au)	$E_{corrected}$ (au)	$E_{counterpoise}$ (kcal)	$E_{binding}$ (kcal)	n−π* (eV)	n−π* (nm)	calcd shift (cm^{-1})
pyrazine	−263.6308820				3.9464	314.17	0
one ethane	− 79.5716712						
two ethanes	−159.1452831	−159.1443838	+ 0.56	−0.65			
1a	−343.2075516	−343.2047708	+ 1.74	−1.39	3.9431	314.44	−27.3
1b	−343.2079637	−343.2049077	+ 1.92	−1.48	3.9411	314.59	−42.5
2a	−422.7851534	−422.7791990	+ 3.74	−3.12	3.9389	314.77	−60.7
2b	−422.7848694	−422.7791997	+ 3.56	−3.12	3.9419	314.53	−36.4
2c	−422.7848424	−422.7790330	+ 3.64	−3.02	3.9403	314.66	−49.6
2d	−422.7843217	−422.7790769	+ 3.29	−3.04	3.9395	314.72	−55.6
3	−502.3622435	−502.3535328	+ 5.47	−4.79	3.9398	314.69	−52.6
4	−581.9393952	−581.9278913	+ 7.22	−6.48	3.9361	315.00	−83.9

TABLE 2: Predicted Supercritical Ethane Bulk Densities for Pyrazine Solvation Shell Average Occupancy by One, Two, Three, and Four Ethanes

ethane no.	calcd n−π* shift (cm^{-1})	exptl n−π* shift[a] (cm^{-1})	predicted density (g cm^{-3})
1	−34.9	−50.0	0.0635
2	−50.6	−61.3	0.0875
3	−52.6	−65.5	0.0915
4	−83.9		0.129 (35.0 °C)
			0.150 (55.0 °C)

[a] Reference 35.

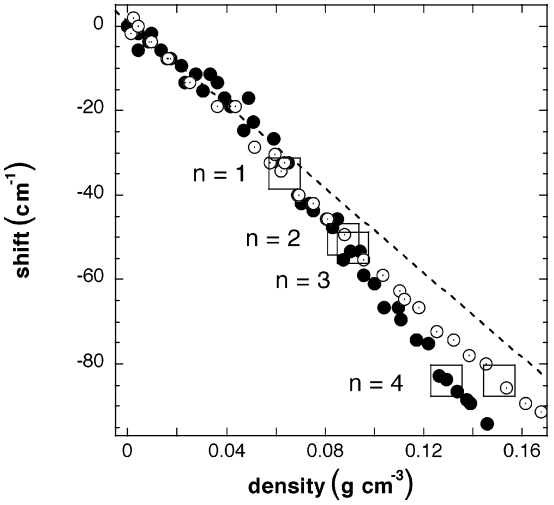

Figure 11. Ethane bulk density predictions for the average of one, two, three, and four ethanes in the pyrazine primary solvation sphere. Predictions (open squares, n = ethane number) superposed on low-density plot expansion of the red shift of the 0−0 band maximum of the pyrazine n−π* transition as a function of ethane bulk density (see Figure 4) at 35.0 (filled circles) and 55.0 (open circles with center dot) °C.

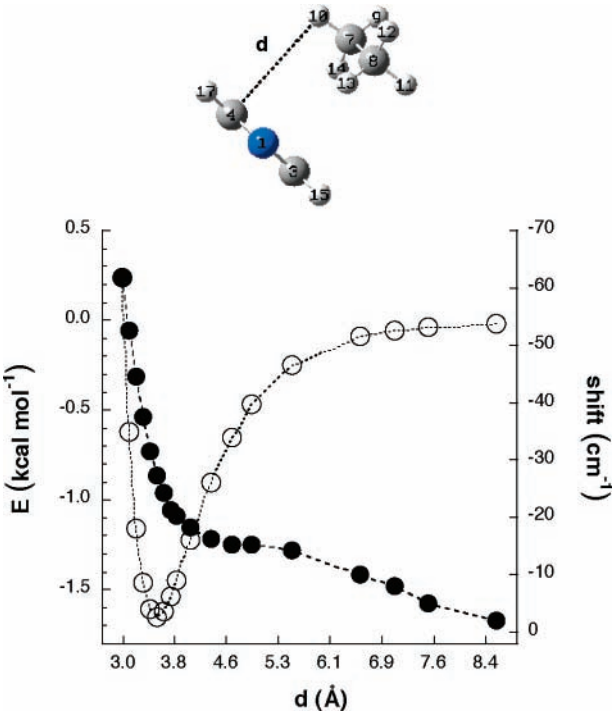

Figure 12. Energy and calculated n−π* shift of **1c** as a function of pyrazine−ethane distance. The distance coordinate (d) is a line perpendicular to the pyrazine plane and defined by C4 of pyrazine and H10 of ethane. Open circles indicate the energy as a function of intermolecular distance. Filled circles indicate the shift in calculated n−π* transition relative to isolated pyrazine as a function of intermolecular distance.

the presence of counterpoise for van der Waals clusters of this type if high accuracy is required. The effects of BSSE on geometry optimization are well-studied in hydrogen-bonded systems,[53] and also studied in systems in which dispersion plays a large role.[54]

Frequency calculations at the MP2/6-311++G(d,p) level for refined structure **1c** and isolated pyrazine and ethane afforded vibrational zero-point energies (ZPE) of 95.63, 47.78, and 47.53 kcal mol^{-1}, respectively. The change in ZPE on formation of **1c** (ΔZPE) is therefore 0.31 kcal mol^{-1}. This gives an estimated $\Delta H°$ of formation for **1c** of −1.34 kcal mol^{-1}. The frequency calculation for **1c** also allowed identification of a low-frequency vibrational mode (62.72 cm^{-1}) that corresponds to a pyrazine−ethane intermolecular stretching vibration. We also calculated the single-point energy of the refined structure **1c** at the MP2 level of theory with a large basis set (aug-cc-pVQZ) known to be near the basis set limit for van der Waals clusters of this type.[28,29] The BSSE corrected binding energy at this basis set size is −2.42 kcal mol^{-1}, for which the counterpoise correction decreases to 0.31 kcal mol^{-1}. Since the MP2 method probably overestimates the binding energy for a dispersion dominated system of this type, it is likely that we have bracketed the **1c** binding energy (−1.65 to −2.42 kcal mol^{-1}).

Probe of Structure 1c Potential Surface. One might expect the pyrazine−ethane potential surface to be rather flat. We probed this surface by choosing a convenient coordinate within refined structure **1c** and calculating the energy of the system as a function of pyrazine−ethane distance (Figure 12, see also Supporting Information, Table 1S) and rotation of ethane with respect to pyrazine at the bottom of the **1c** potential well (Figure 13, see also Supporting Information, Table 2S). The convenient coordinate is a line defined by C4 of pyrazine and H10 of ethane (arbitrary labels assigned by Gaussian03 input files). The line defined by these two atoms (d = 3.54624 Å) is very nearly perpendicular (90 ± 1°) to the pyrazine plane. Variation in C4−H10 distance from about 3 to 9 Å with all other parameters

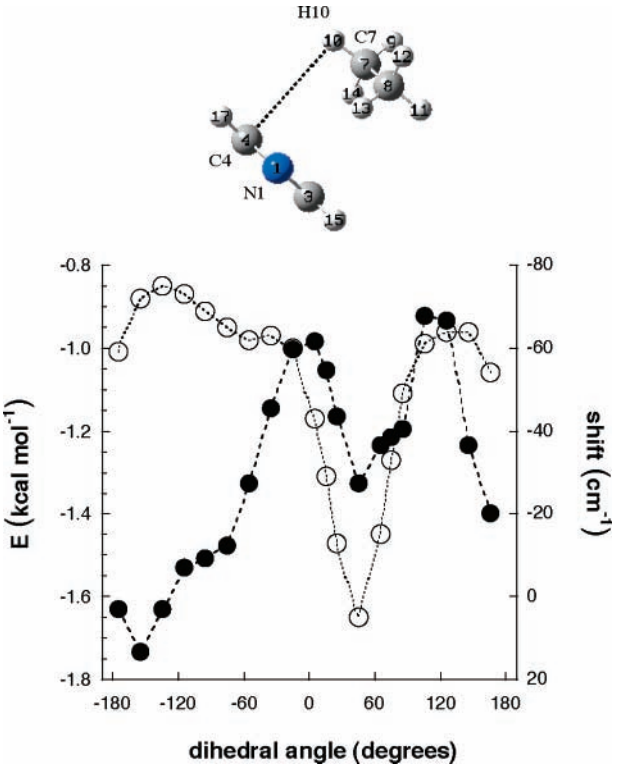

Figure 13. Energy and calculated n−π* shift of **1c** as a function of full 360° rotation about the C7−H10−C4−N1 dihedral angle. Open circles indicate energy as a function of rotation of ethane with respect to fixed pyrazine at the bottom of the **1c** potential well. Filled circles indicate shift in calculated n−π* transition relative to isolated pyrazine as a function of this rotation.

held constant gave calculated binding energies (MP2/6-311++G-(d,p), counterpoise corrected) that show behavior consistent with a typical intermolecular potential (Figure 12). This attractive potential well extends nearly 6 Å. We defined a dihedral angle (45.23°) for rotation of ethane with respect to pyrazine that includes the intermolecular line C4−H10 and incorporates C7 of ethane and N1 of pyrazine (Figure 13). A full 360° rotation about this C7−H10−C4−N1 dihedral angle with all other parameters held constant gave binding energies (MP2/6-311++G-(d,p), counterpoise corrected) that reveal the shallowness of the **1c** potential well. All geometries achieved by rotation about the C4−H10 axis are attractive. About two-thirds of this rotational surface is very flat, and the binding energy varies between −0.85 and −1.06 kcal mol^{-1}. The remaining one-third of this rotational surface includes the potential minimum for **1c** and is approximately symmetrical with respect to this minimum. Rotation from a dihedral of about 0° to 125° corresponds to structures in which the ethane is poised above the pyrazine plane for maximal interaction with the π system.

Figures 12 and 13 also depict our TDDFT/B3LYP/6-311++G(d,p) results, in terms of calculated n−π* transition shift relative to isolated pyrazine, for each of the structures obtained by variation in C4−H10 distance and C7−H10−C4−N1 dihedral angle. We thereby probed the sensitivity of the shift to change in intermolecular distance and rotation within the **1c** potential well. Compression of the intermolecular distance (Figure 12) from the potential minimum to the point at which the interaction becomes repulsive results in a near doubling of the magnitude of the red shift. Increase in the intermolecular distance from the potential minimum at about 3.5 Å to 9.0 Å results in a steady decline in the magnitude of the red shift to near zero. Rotation of ethane about the C4−H10 intermolecular axis (Figure 13) is bimodal; the magnitude of the red shift approximately doubles at the two dihedral angles in which the C7−H10 bond of ethane eclipses an N−C bond (dihedral 0°) and a C−C bond (dihedral 124.8°) of pyrazine. The n−π* shift even moves slightly to the blue (+13.2 cm^{-1}), but not at dihedral angles for which a hydrogen of ethane is in close proximity to the region occupied by a nitrogen lone pair. Rather, this blue-shift region corresponds to rotamers that have the smallest overlap between ethane and the pyrazine π system and in which the ethane is most remote from nitrogen atoms. At this early stage in our exploration of the pyrazine−ethane potential surface, we can conclude that the structure has access to many ground-state geometries whose n−π* shifts range from about −67.7 to +13.2 cm^{-1}. We predict a population maximum at a shift of −27.3 cm^{-1}, the **1c** potential minimum. Given the experimentally observed 0−0 band broadening with increasing ethane density (see Figures 2 and 4), this is not surprising.

Structure **4** for pyrazine and four ethanes (see Figure 10) reveals that perhaps there is adequate room for two additional ethanes in the pyrazine primary solvation sphere where their interactions with the pyrazine π system could induce continued shift to the red. Beyond six ethanes, it would seem that additions to the primary solvation sphere would not have much of an effect on the n−π* transition. Indeed, an ethane bulk density of about 0.2 g cm^{-3} (at 35.0 °C) is qualitatively the point at which the rate of change in shift with respect to density seems to diminish markedly (see Figure 6). We suggest that continued red shift in the higher density regime from 0.3 to 0.4 g cm^{-3} is not the result of a long-range continuum effect. Rather, it may be the result of constriction[52] of the primary solvation sphere, which is a consequence of populating the secondary, tertiary, and higher solvation shells. The red shift is very sensitive to compression of the pyrazine−ethane intermolecular distance; a mere 0.5 Å compression doubles the magnitude.

Conclusion

We predict supercritical ethane bulk densities at which the pyrazine primary solvation sphere is populated by an average of one, two, three, and four ethanes using a combined experimental and quantum chemical approach. Low-temperature supersonic expansion data[35] for pyrazine−ethane clusters lend credence to our predictions. We further suggest that the continued n−π* shift to the red at higher density is the result of primary solvation sphere compression, and not the result of a long-range continuum effect. Simulations based on accurate potentials for pyrazine−ethane and ethane−ethane interactions will allow confirmation or rejection of our bulk density predictions. If confirmed, simulations will also afford information on the width of these average number density predictions.

This combined experimental and quantum chemical approach to characterize the elusive local density in the highly compressible region of supercritical fluids may prove general. If so, it can be applied to test systems that might include unimolecular photochemical reactions. Eventually, we may apply this approach to more challenging bimolecular reactions that require higher reactant concentrations, for which the phase behavior can no longer be approximated as that of the pure fluid. The ultimate goal is to understand solute behavior in supercritical fluids well enough that they may be used as tools to probe solvent effects.

Acknowledgment. We are grateful to Professors R. Viswanathan and N. Asherie of Yeshiva University for very helpful discussions and for their careful reading of this

manuscript. Mr. J. Delgado provided essential technical assistance. We are especially grateful to Dr. M. Lowengrub and Yeshiva University for generous support of this work.

Supporting Information Available: Calculated ground-state MP2/6-311++G(d,p) energies and excited-state TDDFT/B3LYP/6-311++G(d,p) singlet n−π* transition energies for structure **1c** as a function of pyrazine−ethane distance; calculated ground-state MP2/6-311++G(d,p) energies and excited-state TDDFT/B3LYP/6-311++G(d,p) singlet n−π* transition energies for structure **1c** as a function of 360° rotation of ethane with respect to pyrazine. This material is available free of charge via the Internet at http://pubs.acs.org.

References and Notes

(1) Cramer, C. J.; Truhlar, D. G. *Chem. Rev.* **1999**, *99*, 2161−2200.
(2) Mennucci, B. *J. Am. Chem. Soc.* **2002**, *124*, 1506−1515.
(3) Reichardt, C. *Solvents and Solvent Effects in Organic Chemistry*, 3rd ed.; Wiley-VCH: Wenheim, Germany, 2003.
(4) Hrnjez, B. J.; Mehta, A. J.; Fox, M. A.; Johnston, K. P. *J. Am. Chem. Soc.* **1989**, *111*, 2662−2666.
(5) Tucker, S. C. *Chem. Rev.* **1999**, *99*, 391−418.
(6) Kajimoto, O. *Chem. Rev.* **1999**, *99*, 355−389.
(7) Zhou, S. *J. Phys. Chem. B* **2005**, *109*, 7522−7528.
(8) Lalanne, P.; Tassaing, Y.; Danten, F.; Cansell, S. C.; Tucker, S. C.; Besnard, M. *J. Phys. Chem. A* **2004**, *108*, 2617−2624.
(9) Jitariu, L. C.; Masters, A. J.; Hillier, I. H. *J. Chem. Phys.* **2004**, *121*, 7795−7802.
(10) Saito, K.; Kajiya, D.; Nishikawa, K. *J. Am. Chem. Soc.* **2004**, *126*, 422−423.
(11) Kometani, N.; Takemiya, K.; Yonezawa, Y.; Amita, F.; Kajimoto, O. *Chem. Phys. Lett.* **2004**, 85−89.
(12) Song, W.; Maroncelli, M. *Chem. Phys. Lett.* **2003**, *378*, 410−419.
(13) Yamaguchi, T.; Kimura, Y.; Nakahara, M. *J. Phys. Chem. B* **2002**, *106*, 9126−9134.
(14) Patel, N.; Biswas, R.; Maroncelli, M. *J. Phys. Chem. B* **2002**, *106*, 7096−7114.
(15) Parsons, D. F.; Boone, B. I.; Jessop, P. G.; Tucker, S. C. *J. Supercrit. Fluids* **2002**, *24*, 173−181.
(16) Lewis, J. E.; Biswas, R.; Robinson, A. G.; Maroncelli, M. *J. Phys. Chem. B* **2001**, 3306−3318.
(17) Maddox, M. W.; Goodyear, G.; Tucker, S. C. *J. Phys. Chem. B* **2000**, *104*, 6248−6257.
(18) Nishikawa, K.; Morita, T. *Chem. Phys. Lett.* **2000**, *316*, 238−242.
(19) Song, W.; Biswas, R.; Maroncelli, M. *J. Phys. Chem. A* **2000**, *104*, 6924−6939.
(20) Tucker, S. C.; Maddox, M. W. *J. Phys. Chem. B* **1998**, *102*, 2437−2453.
(21) Møller, C.; Plesset, M. S. *Phys. Rev* **1934**, *46*, 618−622.
(22) Clark, T.; Chandrasekhar, J.; Spitznagel, G. W.; Schleyer, P. v. R. *J. Comput. Chem.* **1983**, *4*, 294−301.
(23) Bauernschmitt, R.; Ahlrichs, R. *Chem. Phys. Lett.* **1996**, *256*, 454−464.
(24) Becke, A. D. *J. Chem. Phys.* **1993**, *98*, 5648−5652.
(25) Weber, P.; Reimers, J. R. *J. Phys. Chem. A* **1999**, *103*, 9821−9829.
(26) Boys, S. F.; Bernardi, F. *Mol. Phys.* **1970**, 553−561.
(27) Kendall, R. A.; Dunning, T. H., Jr.; Harrison, R. J. *J. Chem. Phys.* **1992**, *96*, 6796−6806.
(28) Dunning, T. H., Jr. *J. Phys. Chem. A* **2000**, *104*, 9062−9080.
(29) Tsuzuki, S.; Honda, K.; Uchimaru, T.; Mikami, M.; Tanabe, K. *J. Am. Chem. Soc.* **2000**, *122*, 3746−3753.
(30) Wheatly, P. J. *Acta Crystallogr.* **1957**, *10*, 182−187.
(31) Cradock, S.; Liescheski, P. B.; Rankin, D. W. H.; Robertson, H. E. *J. Am. Chem. Soc.* **1988**, *110*, 2758−2763.
(32) Baba, H.; Goodman, L.; Valenti, P. C. *J. Am. Chem. Soc.* **1966**, *88*, 5410−5415.
(33) Bolovinos, A.; Tsekeris, P.; Philis, J. P.; Pantos, E.; Andritsopoulos, G. *J. Mol. Spectrosc.* **1984**, *103*, 240−256.
(34) Innes, K. K.; Ross, I. G.; Moomaw, W. R. *J. Mol. Spectrosc.* **1988**, *132*, 492−544.
(35) Wanna, J.; Bernstein, E. R. *J. Chem. Phys.* **1986**, *84*, 927−935.
(36) Holroyd, R. A.; Nishikawa, M.; Itoh, K. *J. Phys. Chem. B* **2000**, *104*, 11585−11590.
(37) Lindstrom, L.; Rowe, C.; Guilford, T. *Proc. R. Soc. London B* **2001**, *268*, 159−162.
(38) Pophristic, V.; Goodman, L. *Nature* **2001**, *411*, 565−568.
(39) Jayachandran, J. P.; Wheeler, C.; Eason, B. C.; Liotta, C. L.; Eckert, C. A. *J. Supercrit. Fluids* **2002**, *27*, 179−186.
(40) Jessop, P. G.; Brown, R. A.; Yamakawa, M.; Xiao, J.; Ikariya, T.; Kitamura, M.; Tucker, S. C.; Noyori, R. *J. Supercrit. Fluids* **2002**, *24*, 161−172.
(41) Pople, J. A.; Head-Gordon, M.; Raghavachari, K. *J. Chem. Phys.* **1987**, *87*, 5968−5975.
(42) Friend, D. G.; Ingram, H.; Ely, J. F. *J. Phys. Chem. Ref. Data* **1991**, *20*, 275−347.
(43) See: http://webbook.nist.gov/chemistry/.
(44) *Spartan04* for Macintosh and Windows; Wavefunction, Inc.: Irvine, CA.
(45) Frisch, M. J.; Trucks, G. W.; Schlegel, H. B.; Scuseria, G. E.; Robb, M. A.; Cheeseman, J. R.; Montgomery, J. A., Jr.; Vreven, T.; Kudin, K. N.; Burant, J. C.; Millam, J. M.; Iyengar, S. S.; Tomasi, J.; Barone, V.; Mennucci, B.; Cossi, M.; Scalmani, G.; Rega, N.; Petersson, G. A.; Nakatsuji, H.; Hada, M.; Ehara, M.; Toyota, K.; Fukuda, R.; Hasegawa, J.; Ishida, M.; Nakajima, T.; Honda, Y.; Kitao, O.; Nakai, H.; Klene, M.; Li, X.; Knox, J. E.; Hratchian, H. P.; Cross, J. B.; Bakken, V.; Adamo, C.; Jaramillo, J.; Gomperts, R.; Stratmann, R. E.; Yazyev, O.; Austin, A. J.; Cammi, R.; Pomelli, C.; Ochterski, J. W.; Ayala, P. Y.; Morokuma, K.; Voth, G. A.; Salvador, P.; Dannenberg, J. J.; Zakrzewski, V. G.; Dapprich, S.; Daniels, A. D.; Strain, M. C.; Farkas, O.; Malick, D. K.; Rabuck, A. D.; Raghavachari, K.; Foresman, J. B.; Ortiz, J. V.; Cui, Q.; Baboul, A. G.; Clifford, S.; Cioslowski, J.; Stefanov, B. B.; Liu, G.; Liashenko, A.; Piskorz, P.; Komaromi, I.; Martin, R. L.; Fox, D. J.; Keith, T.; Al-Laham, M. A.; Peng, C. Y.; Nanayakkara, A.; Challacombe, M.; Gill, P. M. W.; Johnson, B.; Chen, W.; Wong, M. W.; Gonzalez, C.; Pople, J. A. *Gaussian03*, Revision C.02; Gaussian, Inc.: Wallingford CT, 2004.
(46) Ransil, B. J. *J. Chem. Phys.* **1961**, *34*, 2109−2118.
(47) Rowley, R. L.; Yang, Y.; Pakkanen, T. A. *J. Chem. Phys.* **2001**, *114*, 6058−6067.
(48) Myers, A. B.; Birge, R. R. *J. Chem. Phys.* **1980**, *73*, 5314−5321.
(49) Myers, A. B. *Annu. Rev. Phys. Chem.* **1998**, *49*, 267−295.
(50) Tsuzuki, S.; Honda, K.; Uchimaru, T.; Mikami, M. *J. Chem. Phys.* **2004**, *120*, 647−659.
(51) Tsuzuki, S.; Uchimaru, M.; Mikami, M.; Tanabe, K. *J. Phys. Chem. A* **1998**, *102*, 2091−2094.
(52) Manjari, S. R.; Kim, H. J. *J. Chem. Phys.* **2005**, *123*, in press.
(53) Simon, S.; Bertran, J.; Sodupe, M. *J. Phys. Chem. A* **2001**, *105*, 4359−4364.
(54) Tarakeshwar, P.; Kim, K. S.; Kraka, E.; Cremer, D. *J. Chem. Phys.* **2001**, *115*, 6018−6029.